Ganilova, O. A. and Awaludin, A. and Dong, R. (2017) Hybrid energy harvesting based on cymbal and wagon wheel inspiration. Journal of Intelligent Material Systems and Structures. pp. 1-22. ISSN 1530-8138 (In Press) ,

This version is available at http://strathprints.strath.ac.uk/60191/

Corresponding Author: Dr Olga Ganilova, Department of Mechanical and Aerospace Engineering, University of Strathclyde, Glasgow, G1 1XJ, olga.ganilova@strath.ac.uk

Hybrid Energy harvesting based on cymbal and wagon wheel inspiration

Ganilova[1] O.A., Awaludin[2] A., Dong[2] R.
[1]Department of Mechanical and Aerospace Engineering, University of Strathclyde, Glasgow, G1 1XJ
[2]Department of Mechanical Engineering, University of Sheffield, Sheffield, S1 3JD

Abstract: The demand for self-sufficient electronic devices is increasing as well as the overall energy use, and such demands are pushing technology forward, especially in effective energy harvesting. A novel hybrid Energy Harvesting System (EHS) has been proposed and analysed in this paper. It has been demonstrated that the EHS is capable of converting enough energy to power a typical MEMS device. This has been achieved through unification of the nine Cymbal Energy Harvester (CEH) array, as an energy harvesting core, and Shape Memory Alloy (SMA) active elements, acting as a source of force stimulated by the environmental changes. A Finite Element Model (FEM) was developed for the CEH, which was verified and used for the analysis of CEH's response to the change of the end-cap material. This was followed by the FEM for the EHS used for analysis of the location of SMA wires and force generated by each wire individually and then all together. As a further optimisation of the EHS a novel Wagon Wheel design was explored in terms of its energy harvesting capabilities. As expected, due to the increased displacement, an increase in the power output was achieved.

Keywords: Cymbal, Wagon Wheel, Energy Harvesting, SMA

1. Introduction

As discussed in detail in (Ganilova et al., 2011) the 'Cymbal' Class V flextensional transducer (Tressler et al., 1999) is one of the most widely used miniaturised transducers. The design of this transducer represents a modification of the 'Moonie' transducer (Meyer et al., 2002; Ochoa et al., 2005) with the purpose of increase of the amplification of the piezoceramic disc with the use of additional end caps. Due to their inexpensive fabrication processes, both the moonie and cymbal have become very popular in a number of application areas, namely for towed undersea arrays, fish finders, geophysical research (Meyer et al., 2002), non-invasive drug delivery (Snyder et al., 2006; Park et al., 2007), shape controllers and precision micropositioners (Fernandez et al., 1998), and underwater sound projectors and receivers (Dogan et al., 2004).

Typically, a piezoceramic disc or ring (System 1) is sandwiched between two end-caps (System 2), amplifying the radial motion of the piezo-driver (Figure.1).
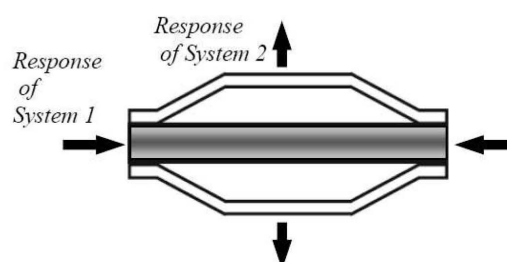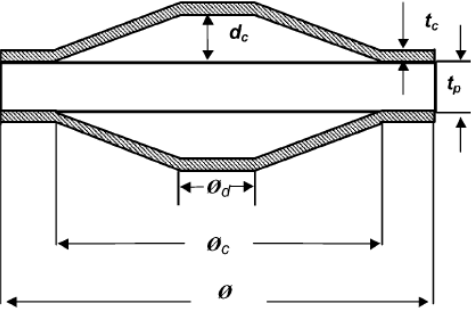

Fig. 1. Cymbal flextensional transducer (Ganilova et al., 2011);

The core material can range from piezoelectrics and electrostrictors to ferroelectric phase switchers or even magnetostrictive materials (Meyer et al., 2002). The choice of the piezoeceramic material and its influence on the structural behaviour have been extensively studied in (Fernandez et al., 1998; Dogan et al., 2004; Meyer et al., 2001; Wang et al., 2006; Lam et al., 2006; Tressler and Howarth, 2002 and Dong et al., 2002). Another widely investigated parameter is the selection of end-cap material which may range from titanium (Meyer et al., 2001), brass (Fernandez et al., 1998), kovar (Ochoa et al., 2005), and tungsten or steel (Meyer et al., 2002; Fernandez et al., 1998; Dogan et al., 2004; Tressler and Newnham, 1997). By studying the effect of the Young's Modulus of the end-cap it was found in Fernandez et al., (1998) that the stiffness of the metal reduces the displacement of the end-cap but allows the structure to support a higher load. As a rule the end-caps are bonded to the driver using a high strength insulating epoxy. To avoid the formation of microcracks and debonding, the epoxy should be able to withstand stresses caused by compression of the piezoeceramics and tension induced by the end-cap. Special care should be taken whilst fabricating to avoid any variation in the epoxy layer thickness since this may cause asymmetry and as a consequence affect the behaviour of the structure. Cymbal behaviour can also be distorted by pronounced asymmetry due to a difference in cavity depth of the end-caps (Meyer et al., 2002; Tressler and Newnham, 1997) and the diameter of the cymbal, which may vary from 40×10^{-3}m down to 3×10^{-3}m, altering the resonance frequencies from 1 kHz to over 100kHz.

Examples of the influence of the cymbal geometry are summarised in the Table 1.

Table 1. The effect of the cymbal geometry

Geometry of cymbal transducer defined in (Dogan, 2004).	Increased dimensions	Results
	Cavity depth d_c	Decrease in displacement and increase in device stiffness
	Device diameter Φ	Increase first resonance frequency
	Cavity diameter Φ_c	Increase first resonance frequency
	End cap thickness t_c	Increase in stiffness and first resonance frequency
	PZT thickness t_p	Increase in stiffness and first resonance frequency

Inspired by the success of the invention of the cymbal transducer based on a novel application of the piezoceramics, researchers proposed subsequent modifications and applications (Zhang et al., 2001; Zhang et al., 1999) increasing even further the displacement of the end-caps (Dong et al., 2002; Sun et al., 2006; Juuti et al., 2005), reducing stresses in the end-caps, and exhibiting a less hysteretic behaviour (Narayaman and Shwartz, 2010). One of the advanced versions of the cymbal transducer is the wagon wheel (Figure. 2), which was developed from the cymbal. The improvement was made by cutting pie-shaped slots on the end cap of the cymbal, thereby reducing the concentration of stress. Therefore the tangential stress on the end caps is reduced so that the mechanical energy otherwise wasted in the cymbal transducer's end cap can be converted into electrical energy.
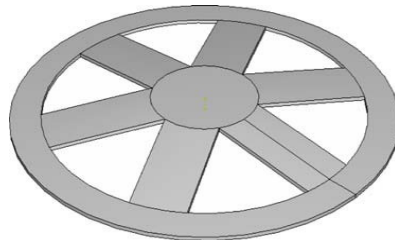
Figure 2. 3D view of wagon wheel with six slots (Narayaman and Shwartz, 2010)

The wagon wheel has the potential for development by changing the number of slots. It was found using finite element analysis of the cymbal that the flexural motion of the end cap would result in a high circumferential stress (Yuan et al., 2009).

The general success of the Cymbal design for transducers has now inspired an additional application for Cymbal design-energy harvesting. Considering the fact that a piezoelectric disc is characterised by the direct and converse piezoelectric effects, this is one of the natural applications for a piezoelectrically characterised transducer.

A typical output for a cymbal energy harvester (CEH) can be found in (Dogan et al., 1997; Kim et al., 2004 and Berlincourt and Krueger) and summarised in Table 2.

Table 2. Experimental results for CEH varying the material of the end-cap

End cap material	Notation	Brass	Brass	Steel	Steel	Steel
End cap dimensions ($\times 10^{-3}$m)	Φ	12.7	29	29	29	29
	Φ_d	3	5	5	5	5
	d_c	0.2	0.3	1	1	1
	Φ_c	9	17	17	17	17
	t_c	0.3	0.3	0.3	0.3	0.3
Piezoelectric material properties		PZT 5A	PI	APC850	D210	APC841
Dielectric constant	ε_r	N/A	N/A	1750	681	1350
Piezoelectric constant	$d_{31}(10^{-12}$ C/N)	171	N/A	175	120	109
	$d_{33}(10^{-12}$ C/N)	374	N/A	400	276	300
	$d_{31}^2/\varepsilon\varepsilon_0(10^{-12})$	N/A	N/A	1.97	2.4	0.99
Force applied (N)		15	51	7.8	7.8	7.8
Frequency applied (Hz)			70	100	100	100
Voltage obtained (V)		100	12	178	260	374

It is worth pointing out that typically, the CEH's behaviour has been described from the basis of experimental data and the resonance frequency is typically of the order of hundreds of Hertz in order to obtain a reasonable output voltage. Nevertheless, to the best of the authors' knowledge, the wagon wheel has not yet been investigated in terms of its energy harvesting potential.

Another relatively recent development has been the investigation of the combination of two smart materials in which they can compliment each other's properties to increase the energy output, and exploit a combination of physical effects, generally extending the area of application. It has been found that there have been a few

attempts to combine shape memory alloys (SMAs) and piezoelectric materials and this work has shown some positive results. In (Zakharov et al., 2012) a simple cantilever unimorph beam was fixed at one end, and attached at the free end to a spring and an SMA. Upon heating the SMA acts as an actuator by providing force at the end of the cantilever which results in a bending motion that produces electrical charge in the PZT. The process results in the conversion of 75 µJ of energy due to a single temperature variation of 60C.

The use of SMA in a cymbal design transducer has been studied in (Feeney & Lucas, 2014). The study proposed the use of SMA as the material for the end cap to provide the cymbal transducer design with a better tuning ability. By using SMA as the material of an end cap, the resonance frequency of the cymbal design energy harvester can be altered to suit multiple operating frequencies. However this study exploited only the potential of the SMA application in a cymbal, operating as a transducer.

It is worth mentioning that according to (SAES Group, 2014) the thermal activation of SMA can result in up to 100N dependent on the shape of the SMA element as a spring, wire, or foil etc with activation time of around 1s (resulting in 0.5-1Hz operating frequency). However there is some evidence in the literature that it is possible to develop a high frequency SMA with an operational frequency of up to 100 Hz (Teh et al., 2007) and even 2kHz (Teh et al., 2005), and this makes it a perfect candidate for energy harvesting from, say, the circulation of a fluid of variable temperature.

The work in this paper concentrates on the **novel** idea of the combination of two smart materials, SMA and PZT, in order to exploit the optimal potential of the cymbal shape for energy harvesting. **For the first time** the combination of the Cymbal energy harvester array together with SMA actuators has been explored in terms of its energy harvesting potential. An optimisation of the introduced novel harvester has been performed, investigating, for the first time, the energy harvesting ability of the wagon wheel design.

2. Description of a novel Energy Harvesting System (EHS) based on the hybridisation of PZT and SMA

The main concept of the design is to utilise the actuation force from the SMA actuator and then to transfer the linear SMA motion into the end caps with minimal losses within a small package. The proposed design consists of nine CEHs that are sandwiched in between metal plates. A number of SMA wires are placed along each of the plate sides to provide the actuating force for the CEHs. The CEHs are connected in series to increase the power generated per cycle (Sun et al., 2013) therefore compensating for the low frequency motion generated by the SMA.

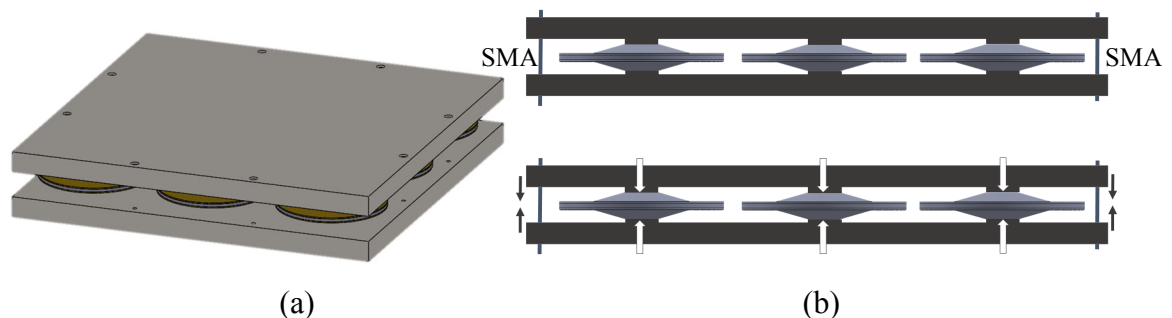(a)   (b)

Figure 3. Representation of the novel hybrid EHS: (a) a 3D view; (b) side view.

A pair of stiff plates is used to hold the CEHs together. The plates provide support and also transfer the actuation force from the SMAs to the CEHs. The plates have dimples at the points where the cymbals are mounted using epoxy in order to ensure that the force is transferred to the tip of the cymbals. The plate sides also have holes where the SMAs wires are mounted.

The top and bottom sides of the plates are coated with a heat conductive metal such as copper or aluminium to assist heat transfer for the SMA wires. The location and number of SMA wires is to be modelled and analysed to achieve an even distribution of the heat generated SMA compressive force, and thus ensure optimal performance of the EHS.

During the time that the SMAs undergo the temperature increase they are characterised by compressive forces that are amplified due to the cymbal end-cap system and then transferred in the form of displacement to the PZT element of the CEH to produce electrical charge. As the SMAs are cooled they relax and the CEH pushes the constraining plates back into their original state (Figure.4).
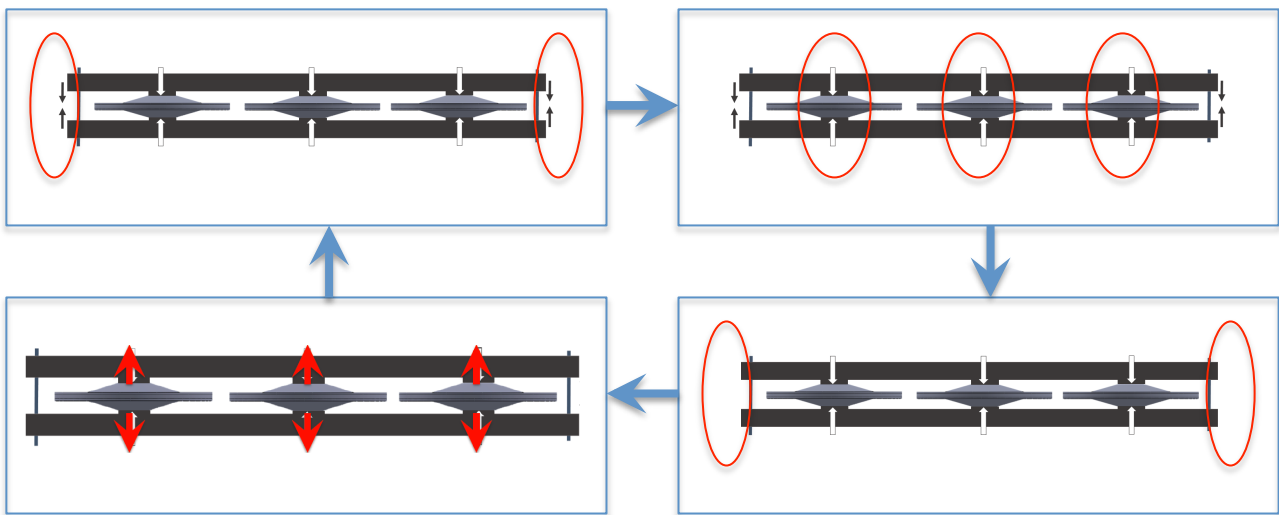

Figure 4. Activation cycle of the SMA

The cyclical nature of the process will result in the vibration of the PZT disc and the production of an AC voltage. This will have to be converted into a DC voltage which can be used directly to power small devices, MEMS, and to recharge batteries directly. The fact that the operating temperature of the SMA (the heating and cooling rate) depends on the composition of the SMA makes it possible to tune/train the SMA wires to be as sensitive as necessary for a specific application.

3. Development and verification of the finite element model of the CEH

A 3-D model has been created using Solidworks and the modelling done by using the commercial package ANSYS 16.0. Mesh convergence has been considered and it was found that the results for the cymbal displacement are not sensitive to the choice of mesh density. Therefore it was decided to choose the auto-mesh tool for the initial investigation.

The chosen boundary conditions are used to represent the motion of the system throughout the process. The faces of the tips of the cymbals have been restricted to execute solely axial motion while the flanges have been similarly restricted but to

radial motion. The displacement measured has the change in thickness and the change in radius of the PZT disc.

The PZT elements in the CEHs are modelled as ceramics and the voltage typically produced by Morgan piezoceramics (Morgan Advanced Materials, 2013) is estimated based on the displacement of the PZT due to the compression as suggested in technical data (Morgan Advanced Materials, 2013). In the novel design of EHS described below (Section 4) the compression will be induced by the SMA wires (the intensity of the force was estimated based on (SAES Group, 2014)). From the displacement of the PZT, the peak voltage produced can be obtained as follows (Morgan Advanced Materials, 2013):

$$V = \frac{\Delta r t}{d_{31} d} \tag{1}$$

$$V = \frac{\Delta t}{d_{33}} \tag{2}$$

where Δr is the change in radius of the PZT, t is the thickness of the PZT, d is the diameter of the PZT, and Δt is the change in thickness of the PZT.

Eq. (1) and Eq. (2) represent the voltage produced due to radial displacement and axial displacement respectively. The values of d_{31} and d_{33} can be obtained from

$$d_{31} = g_{31} . \varepsilon_{r\,33}^{T} \tag{3}$$

where,

$$\varepsilon_{r\,33}^{T} = K_{33}^{T} \varepsilon_0 \tag{4}$$

The maximum output power can be found based on the voltage generated:

$$P = \frac{1}{2} C V^2 \tag{6}$$

where,

$$C = \varepsilon_{r\,33}^{T} \frac{A}{t} = \frac{K_{33}^{T} \varepsilon_0 A}{t} \tag{7}$$

A is surface area and T is the thickness of the piezo-disc (Morgan Advanced Materials, 2013).

The voltage and power output are both dependent on the voltage constant coefficients g_{ij} and the magnitude of the displacement. Since the displacement of the cymbal is in both the d_{31} and d_{33} modes, the combination of the voltages produced depends on the capacitance of the PZT element. The PZT used in the model is of the PZT508 type and its properties can be found in Table 3.

Table 3. Properties of PZT508 based on (Morgan Advanced Materials, 2013).

PZT properties for PZT508		
Density (kg/m^3)	ρ	7900
Poisson's ratio	ν	0.31
Dielectric constant	K_{33}^{T}	3910
	K_{11}^{T}	4048
Strain constants ($\times 10^{-12} m/V$)	d_{33}	744
	d_{31}	3313
Voltage constants ($\times 10^{-3} Vm/N$)	g_{33}	21.5
	g_{31}	9.1

The epoxy layer joining the cymbal end caps and the PZT together is not considered in the model since the layer is extremely thin and is only present under the flange of the end-cap, and is not desirable under the cavity of the dome.

The model simulates the behaviour of the device for a single contraction in the actuation motion of the SMA. Following the typical hysteretic characteristic of SMA behaviour, the relaxing actuation motion is considered to have the opposite effect to the contraction during the cooling process. The combination of both the contraction and relaxation of the SMA represents the SMA operational cycle (Figure.5).
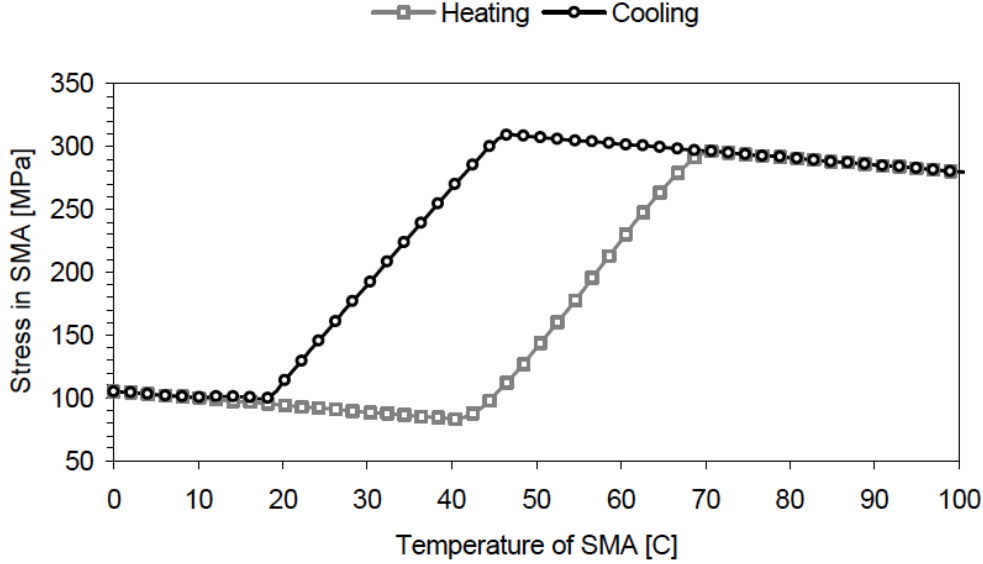

Figure 5. Changes in internal stress of SMA in dependence on the temperature (Ostachowicz et al., 2001).

As can be seen in Figure.5, the behaviour of SMA material can be modelled accurately taking into account the effect of time and temperature. In this case three models could be considered with improved Brinson model being frequently used (Ostachowicz et al., 2001):

$$(\sigma - \sigma_0) = E(\xi)\varepsilon - E(\xi_0)\varepsilon_0 + \Omega(\xi)\xi_s - \Omega(\xi_0)\xi_{0s} + \Theta(T - T_0) \qquad (8)$$

where σ, σ_0 describe stress and initial stress, $\varepsilon, \varepsilon_0$ strain and initial strain, T and T_0 temperature and initial temperature, Θ thermoelastic coefficient. It is assumed that the Young's modulus E, as well as the phase transformation coefficient Ω of a shape memory alloy, are functions of the martensite volume fraction ξ .

However in this paper we are not considering an accurate model for SMA, aiming to provide a maximum power estimate for the design suggested. Therefore SMA output will be estimated at it is maximum (austenite state) in Section 4 (Table 5).

The geometrical parameters of the CEH were chosen bearing in mind the influences of each dimension on the behaviour of the system, i.e. end-caps with a thickness of $0.25 \times 10^{-3} m$ have a higher sensitivity than thicker end-caps (Sun et al., 2006), larger diameter cavities produce larger peak voltage outputs (Wu et al., 2014); a larger cavity with a small dimple increases the deflection of the cymbal end-cap therefore producing large displacements in the PZT. The flange is a crucial point at which the end cap is joined to the PZT in order to transfer displacement. The strength of the joint relies on its surface area. Small area would potentially cause failure in the joints given that they are one of the limiting factors in cymbal transducer design. If the area is too large, it will result in the loss of potential for energy harvesting. In order to validate the model presented in this paper, the dimensions (in Figure 6) were chosen following the experimental work of (Ren et al., 2010). In this work a peak voltage of

15 V and maximum output power of 2.0 mW at a resonance frequency of 650 Hz was achieved.
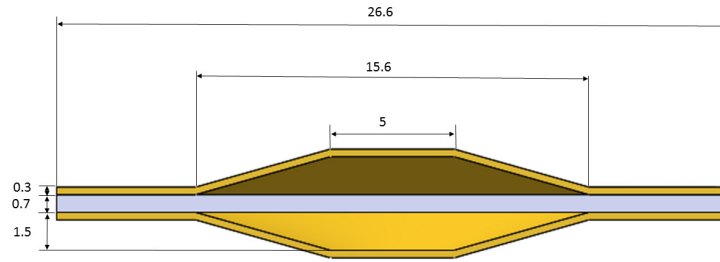

Figure 6. Geometry of CEH (in x10^{-3} m) based on (Ren et al., 2010).

The cymbal was modelled using a brass end-cap for model verification with the work of (Ren et al., 2010). The properties of piezoceramics and the brass end-cap can be found in Tables 3 and 4 respectively.

Table 4. Properties of the End-Cap materials

Material	Density,ρ (kg/m^3)	Young's Modulus, E $(\times 10^9 Pa)$	Poisson's ratio,ν
Brass	8550	100.6	0.35
Titanium	4500	120.2	0.361
Steel	7860	207	0.3

The modelling is concentrated around the study of the behaviour of the cymbal at frequencies ranging from 1 Hz to 100000 Hz. The results are presented in Figure 7 and show the amplitude of the radial and thickness displacements of the PZT within the aforementioned frequencies.
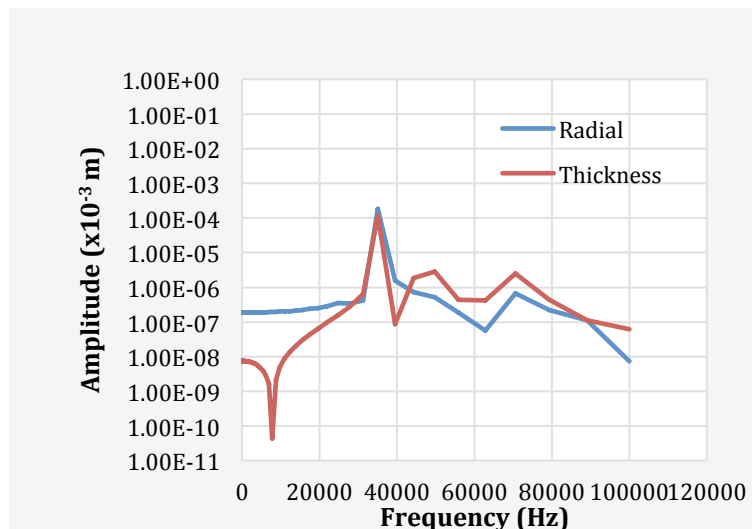

Figure 7. Displacement response of the PZT disc

According to Figure 7 the natural frequency within mode 1 for the PZT disc is found to be at 35112 Hz where the maximum amplitudes were $1.85\times10^{-7}m$ and $1.16\times10^{-7}m$ respectively for the radial and axial displacements. At frequencies lower than the natural frequencies the displacement amplitudes were significantly lower.

The cymbal operates at a lower frequency therefore the amplitude of the PZT disc, and thus that of the whole cymbal, will necessarily be much lower. In order to increase the amplitude of the PZT displacement, the applied force then has to be increased.

A static structural model was developed where the force was varied between 1 to 10N on the tips of the cymbal. In Figure 8 it is possible to observe the deflection of the CEH when the forces are applied at the tips of the cymbal. The model shows that the PZT deformation occurs largely in the region where the PZT adheres to the flange of the end-cap, and this corresponds to the main operating principle of a cymbal device. Minimal deformation occurs at the central region of the PZT at the cavity of the end cap.
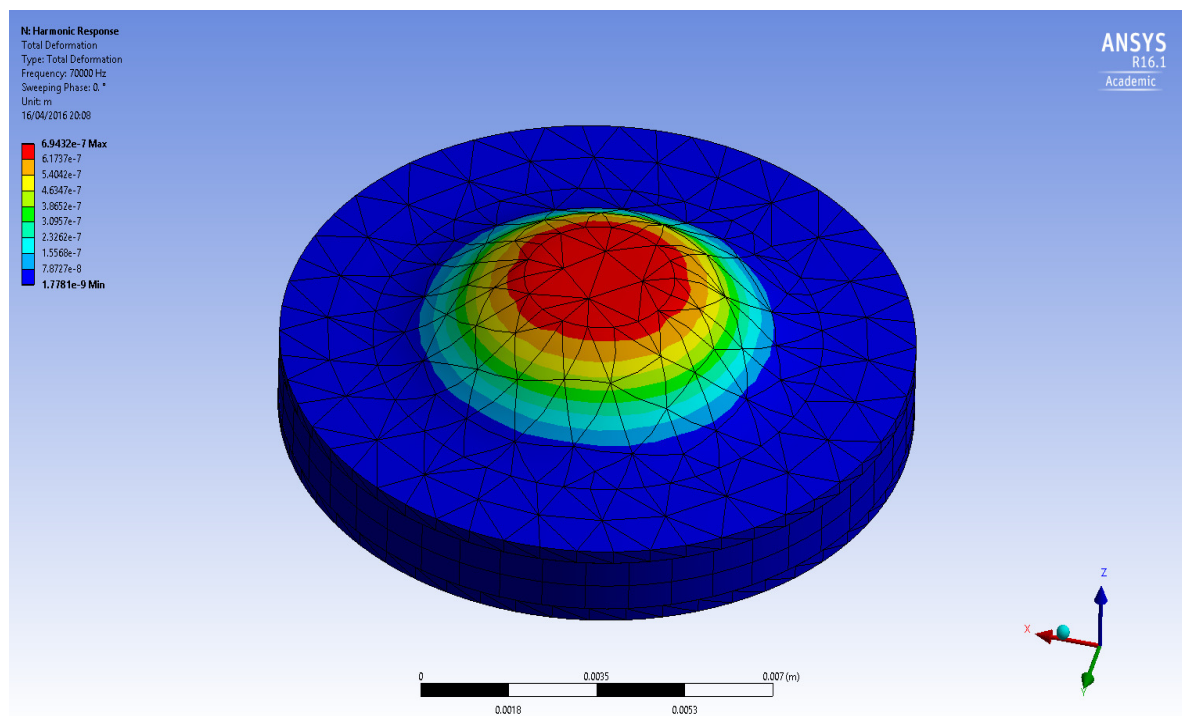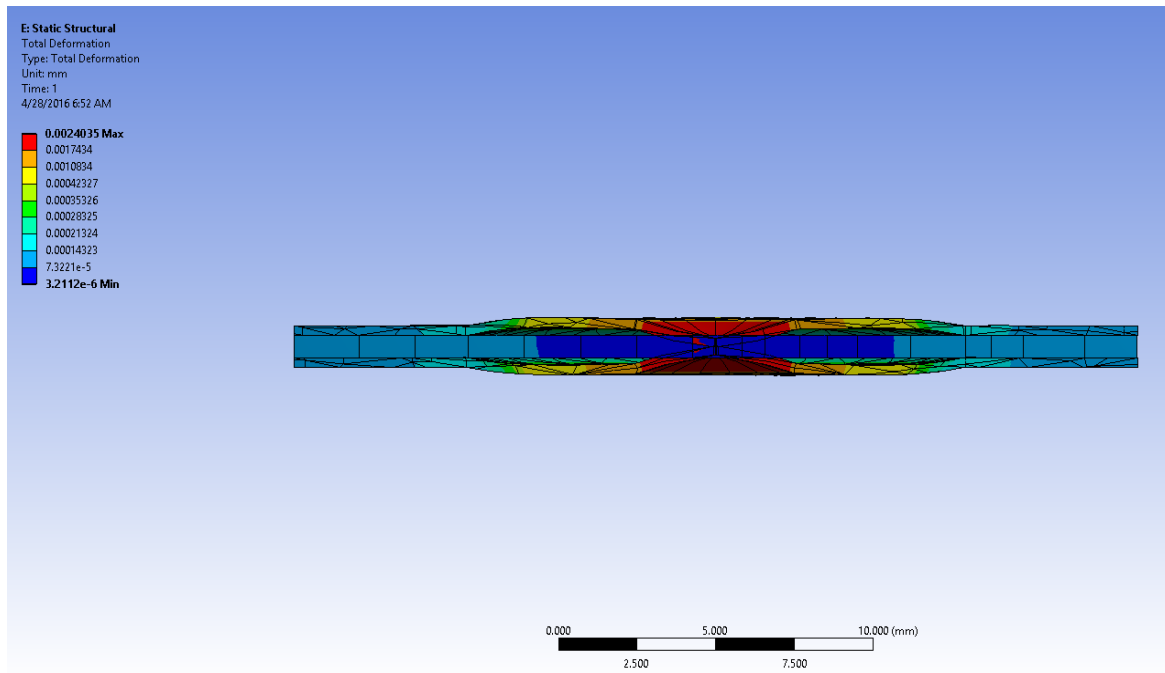
Figure 8. Cymbal transducer behaviour

Based on the response behaviour of the end-cap and the PZT disc the total output voltage can be calculated as presented in Figure 9. It can be noted that the output voltage increases with an increase of the applied force. This reflects the cymbal's operational pattern, so when the force increases then the displacement increases. This results in an increase in peak voltage output and maximum output power.
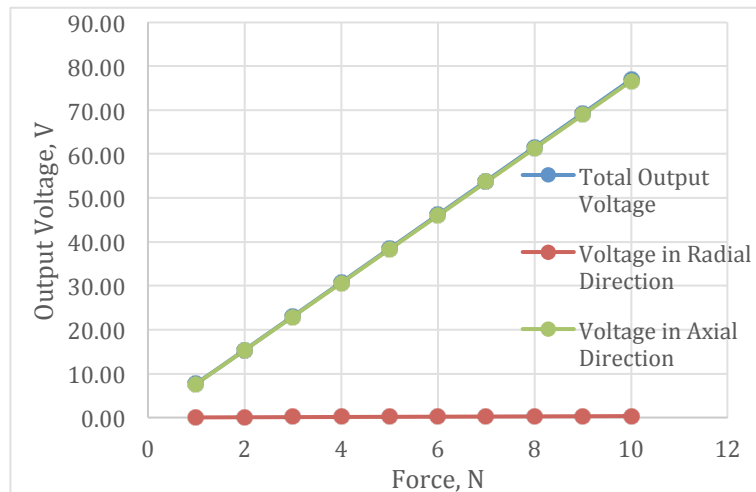

Figure 9. Radially and axially directed voltages produced by the applied force

The results show the proportionality of the output voltage produced to the increasing applied force. The measured displacement was the average radial and axial displacements. The results also show that the output voltage due to the radial displacement (based on d_{31}) is much lower when compared to the output voltage from the axial displacement (based on d_{33}). These results confirm the fact that the CEH converts a large amount of energy due to the axial force generated by the mechanical motion of the end-cap.

3.1.   Effect of the End-Cap Materials

As mentioned in the Introduction it has been found in the literature that the choice of the cymbal end-cap material influences the response of the whole system. Therefore a comparison of the voltage outputs for three CEHs made of steel, titanium and brass (Table 4), and dimensions chosen according to (Ren et al., 2010) and discussed above, has been presented in Figure10.
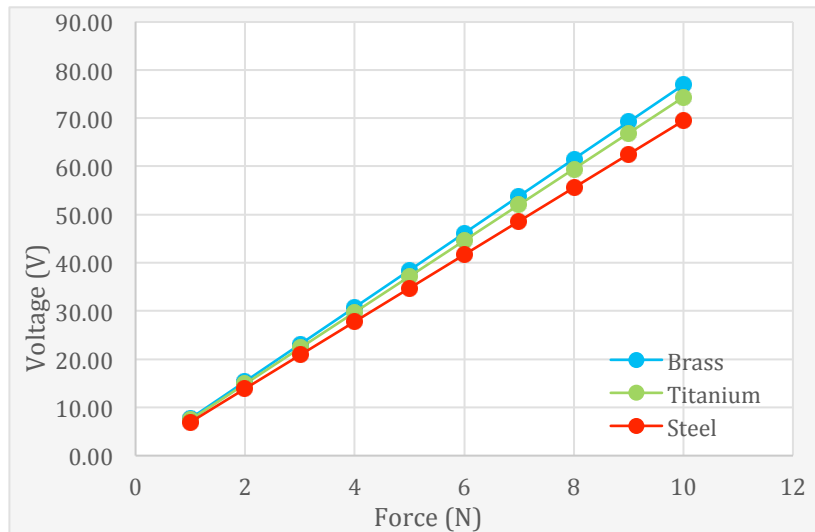

Figure 10. Voltages produced by CEHs using different end-cap materials

As stated in (Fernandez et al., 1998) the response of CEHs with end-caps made of different materials depends principally on the stiffness of the material. The results presented in Figure 10 confirm that the brass end-cap shows the best performance, followed by titanium and then steel. The behaviour is obviously defined by the Young's Modulus, which in turn affects the stiffness properties of the CEH's end-cap, and the displacement as a result.

4. Development of the finite element model (FEM) of the EHS

Nine CEHs are arranged symmetrically in between two plates which sandwich the CEHs as shown in Figure 11 (a)&(b). Due to the stiffness of the plates, during SMA wire contraction the plate deflects. The deflection of the plates results in a different pattern of the force distribution along each cymbal. To simulate this in ANSYS the displacement of the top and bottom plates is unconstrained in the vertical direction due to the compressive force of the SMA and the reactive force of the Cymbals. To represent the force generated by the SMA a distributed force has been applied at the fastener contact points (Figure 3 and 12). The intensity of the force was estimated based on (SAES Group, 2014).
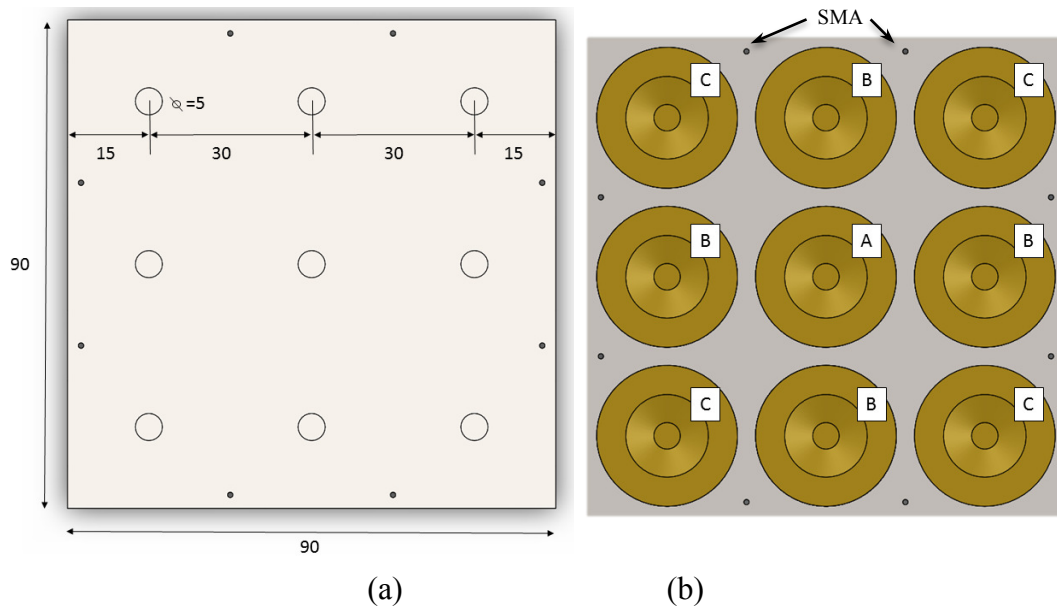
Figure 11. Finite element model of the EHS

Figure 11 describes a specific numerical example of the EHS that is modelled by the FEM. The CEHs are placed on dimples that have a diameter of $5x10^{-3}$ *m* to match the tips of the CEHs. The dimples aid the transfer of forces applied due to plate compression directly on to the tips of the CEHs. The holes on the edges are used to mount the SMA wires. The positions of the holes are considered for Configuration 1 (C1) and Configuration 2 (C2), as presented in Figure 12.
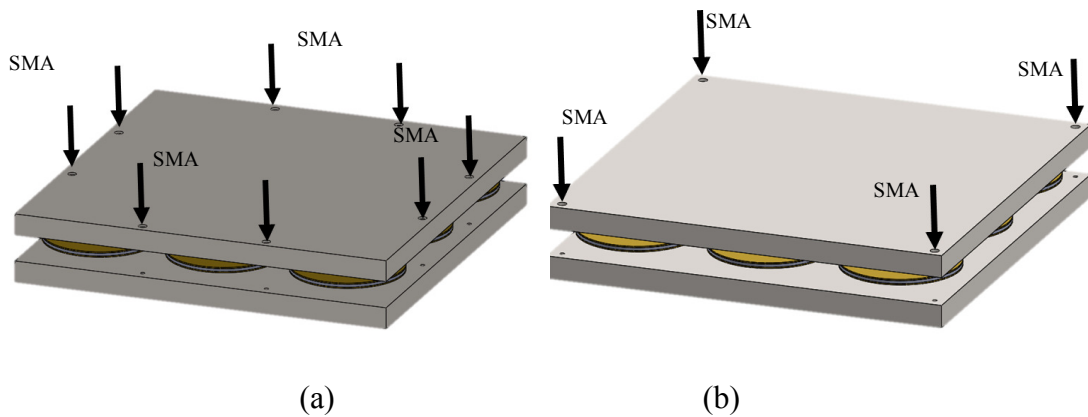
Figure 12. SMA wire locations: (a) Configuration 1 and (b) Configuration 2

Each cymbal in the EHS (Figure 12 (a)) behaves differently due to the uneven deflection of the top and bottom plates, therefore three different measurements have been taken into account. The behaviour of the three different CEHs was analysed due to their different locations A, B, C shown in Figure 11 (b). It is assumed that the CEHs labelled A follow the same pattern of behaviour due to the EHS's symmetry. The same applies to the set of CEHs labelled B and C.

According to (SAES Group, 2014), SMA wires can be provided with crimps to secure them in place. The crimps can be used to support a force of up to 50 N, and this is sufficient for the current design.

Due to the large value of forces produced by the SMA wires, the material and dimensions of the plates have to be chosen appropriately. Therefore for the EHS described here the plates were chosen to be made of steel. This will result in lower buckling of the plates and a more even distribution of the force along the array of CEHs. The plates are also given a heat conductive coating which increases the thermal conductivity of stainless steel by 70% (Espana et al., 2009). This additional coating guarantees the most efficient and fastest heat transfer to the SMA wires.

For the analysis of two configurations presented in Figures 12 four FEMs were created, as described in Table 5. The estimate of force produced by the SMA wires in the austenite phase with an operating temperature of 40°C is based on (SAES Group, 2014).

Table 5. Four models defined by different locations of SMAs according to Figures 10.

Model	Configuration	Number of SMA	SMA Force (N)	
			Each	Total
I	1	8	16	128
II	2	4	16	64
III	2	4	32	128
IV	1	8	32	256

It should be noted that the models were developed by varying the force per SMA wire in each configuration and by simulating half a cycle. The repeating cycles following the frequency of the SMA actuations are considered to be a repetition of this behaviour. The results of the FEM simulations are presented in Figure 13 (a),(b).

(a)   (b)
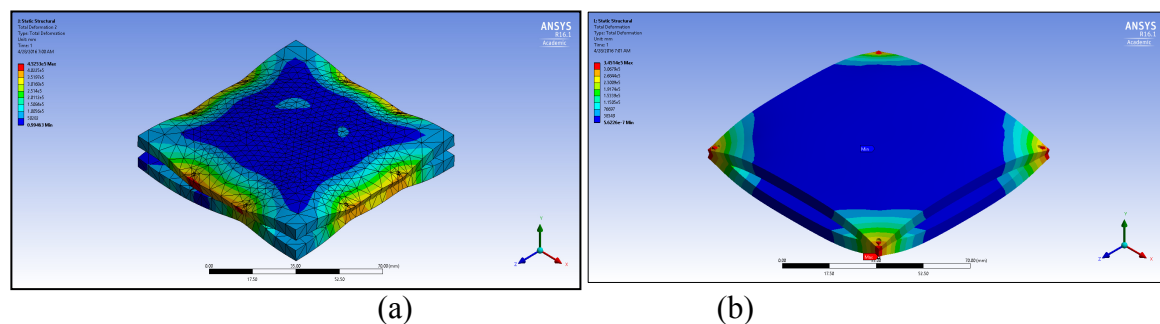
Figure 13. FEMs for Configuration 1 (a) and Configuration 2 (b)

In Figure 13 it can be seen that in the case of Configuration 2 the results show a significantly higher concentration of stress in the corners of the plate, therefore potentially creating buckling in the centre of the plate. This means that the distribution of the force along the CEHs in the central location is significantly reduced.

The analysis of the stress distribution along the array of CEHs for both configurations has been summarised in Figure 14.

Figure 14. Forces acting on the A, B, C CEHs within the four models for C1 and C2

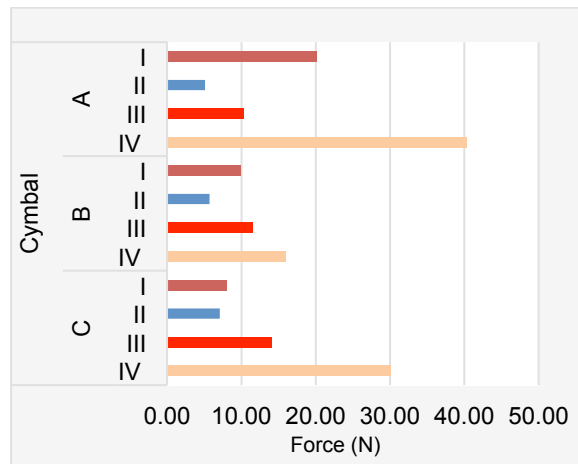The results in Figure 14 demonstrate that Models I and IV transfer a significantly higher force on to the set of CEHs labelled A.

Models II and III, however, exhibit a more equal distribution of the forces being transferred on to the CEHs labelled A, B and C. Cymbals A show a lower force being transferred as compared to the other cymbals. As previously shown in Figure 13, due to the buckling of the plates by the forces in the corners of the plate and supported by the cymbals, the central location of the plates exhibits a large deflection therefore reducing the force that is being transferred to the CEHs labelled A.

The total force generated by the SMA wires within each of the four models considered for C1 and C2 is plotted against the force which is actually transferred to the Cymbals and presented in Figure 15.
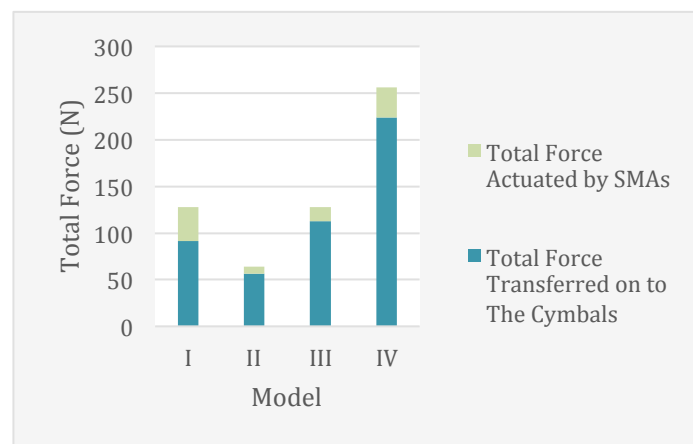
Figure 15. Total force transferred to the cymbals for each model

As can be concluded from Figure 15, model I and model II use SMA wires with the same capacity, but the higher number of SMA wires in model I results in a larger total force being transferred on to the CEHs. However when model I is compared to model III, where the total force of the SMAs is the same, model III results in a larger force being transferred to the CEH. As seen in Figure 15 the percentage of force being transferred to the cymbal transducers in Model I is 72%, as compared to the other models with a higher percentage of 88%. The lower percentage of force transferred is a result of the different behaviours of the plate due to the actuation forces of the

SMAs at different positions and strengths. The lower forces used in Model I are shown to be less effective such that 28% of the effect of the force were lost.

The results show that a lower number of SMAs at different positions is more effective in distributing and transferring the forces on to the cymbals. In addition, the forces were also shown to be distributed more evenly as compared to the alternative configuration where the forces are skewed towards the central cymbal transducer, in cymbal transducer A.

When comparing the use of the same SMA, but with different positions, clearly the configuration with a higher number of SMAs will produce a larger force and that will result in a higher voltage being produced. For maximum harvestable energy output the model with the higher number of SMAs is an advantage.

Using Eqs. (1) and (2), the peak voltage outputs of the different models can be calculated. The two models, model III and IV, with the largest force transferred were compared in Figure 16.
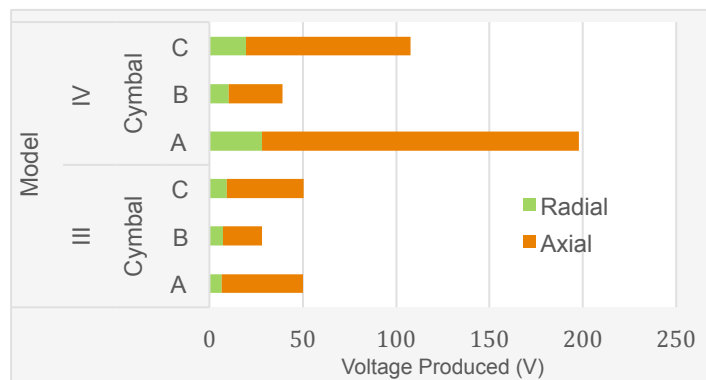

Figure 16. Comparison of voltage output for models III and IV

From Figure 16 it can be seen that model III generates nearly half as much peak output voltage as Model IV. This is due to the fact that model IV has twice the number of SMAs thus producing twice the amount of compressive force. As the force increases, the displacement of the PZT increases therefore increasing the peak output voltage.

5. Optimisation of CEH performance - the Wagon Wheel implementation

Since the Wagon Wheel (WW) transducer is considered to be a significant optimisation of the cymbal transducer but has never been considered in terms of its energy harvesting potential, it is of particular interest to compare its performance as a harvester with that of the CEH. In order to perform this comparison a six-slot wagon wheel energy harvester (WEH) has been modelled (Figure 17).
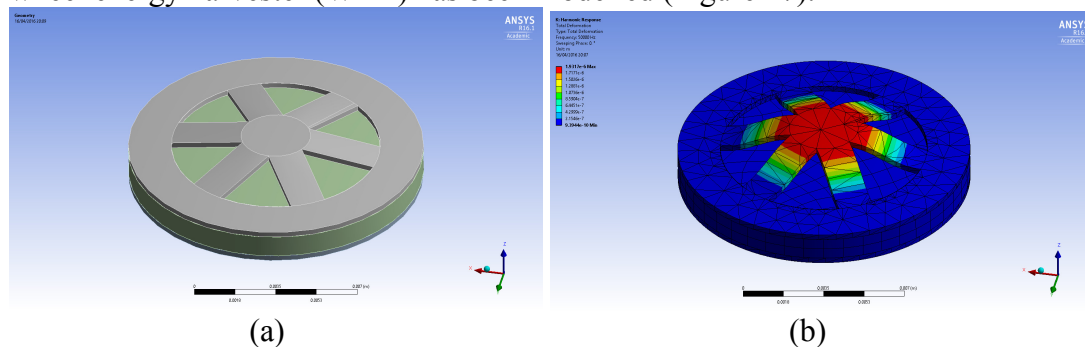

(a)   (b)

Figure 17. Six-slot WEH being modelled

Two other models with four and eight slots have been developed in order to analyse the influence of the number of slots on the energy output of the WEH Figure 18.
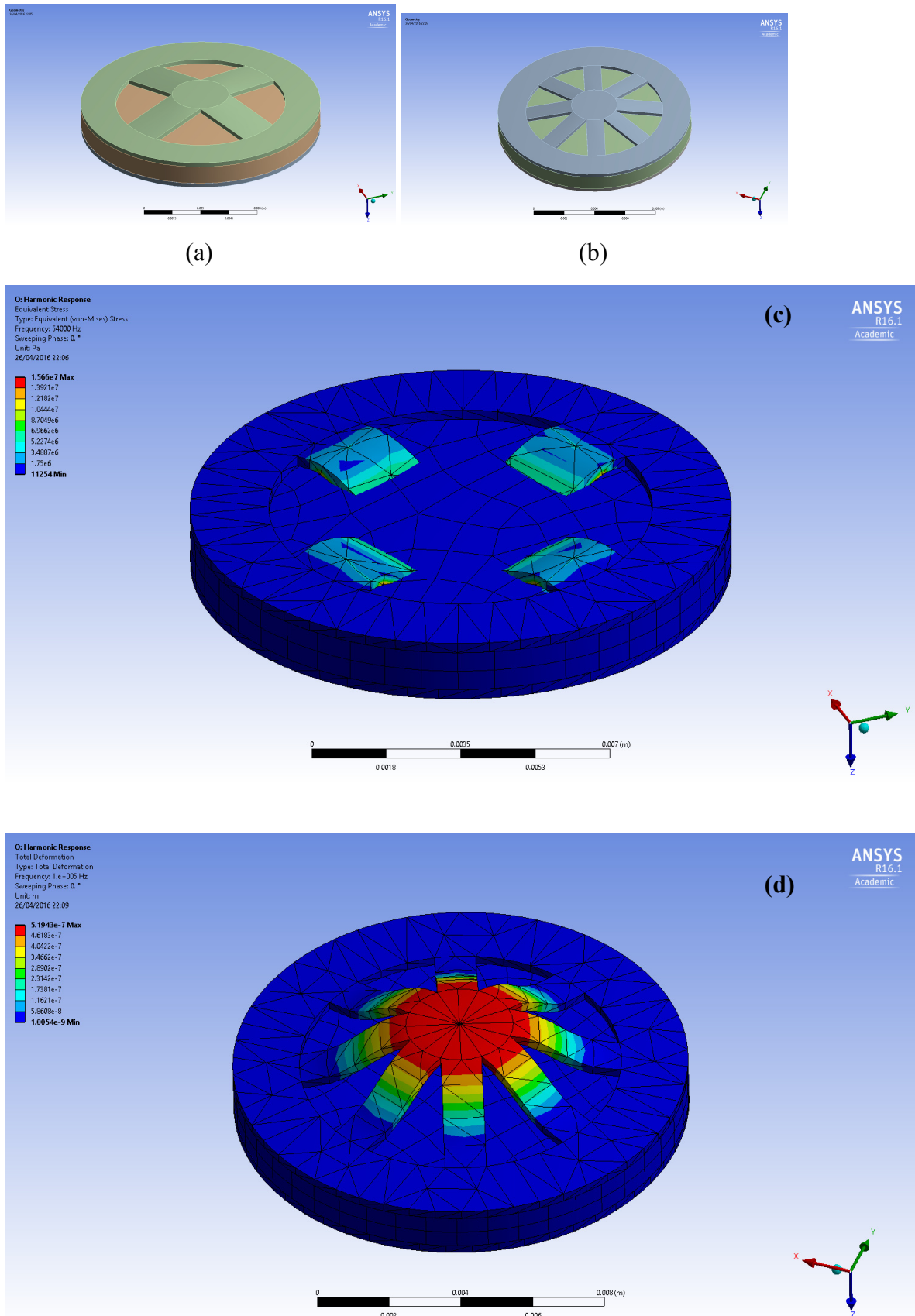

(a)

(b)

(c)

(d)

Figure 18. WEH: Four-slot and Eight-slot: (a), (b) - FEM; (c), (d) - stress distribution

Results in relation to the number of slots and different material for the WEH are summarised in Table 6 in comparison with CEH.

Table 6. Comparison of CEH and WEH performance for different end-cap materials

Endcap Material Properties (Brandes, 1983)	Symbol	Steel	Titanium	Brass
	E (GPa)	207	120.2	100.6
	v	0.3	0.361	0.35
	ρ (kg/m^3)	7860	4500	8500
Endcap Dimensions (x10^{-3} m) (Dogan, 2004).	Φ	12.7	12.7	12.7
	Φ_d	3	3	3
	d_c	0.25	0.25	0.25
	Φ_c	9	9	9
	t_c	0.25	0.25	0.25
PZT Material Properties		BaTiO3	BaTiO3	BaTiO3
	E (GPa)	6020	6020	6020
	v	0.3	0.3	0.3
	ρ (kg/m^3)	1.17E+11	1.17E+11	1.17E+11
Force Applied (N)		1	1	1
Max displacement of endcap flange (m)	**Cymbal**	1.686E-08	5.32E-08	6.839E-08
Max displacement of piezo disc (m)		1.616E-08	5.19E-08	6.701E-08
Piezo disc Resonance Frequency (Hz)		88500	72000	60667
Piezoelectric charge constant (m/V)		1.490E-10	1.490E-10	1.490E-10
Voltage (V)		108.43624	348.4631	449.71812
Max displacement of endcap flange (m)	**Wagon wheel**	3.406E-07	7.6E-07	4.227E-06
Max displacement of piezo disc (m)		3.369E-07	7.61E-07	4.214E-06
Piezo disc Resonance Frequency (Hz)		61500	51000	46000
Piezoelectric strain constant (m/V)		1.490E-10	1.490E-10	1.490E-10
Voltage (V)		2261.0738	5105.369	28281.879

It is possible to conclude from Table 6 that the material with the smallest Young's modulus gives rise to the largest displacement, the lowest resonance frequency, and produces the highest voltage, no matter what the end cap shape is. The WEH was also predicted to perform better than the cymbal, since even steel wagon wheel end caps can produce higher maximum voltages than those of the brass cymbal end cap. It can be noted that one of the ways to tune the resonance frequency is to change the material of the end cap.

Making comparison with the results from the previous publication (Dogan et al., 2004) for a device with the same dimensions, the resonance frequency achieved here is much higher. This is due to a different choice of the PZT disc material. Hence, a variation of the piezoelectric disc material could be used for WEH tuning. Following the work of (Kim et al., 2004) it is also possible to state that the voltage output can be increased due to the applied force, which was as high as 7.8N in the work (Kim et al., 2004).

The analysis of the effect of the number of slots on the displacement of PZT thus voltage produced has been conducted and summarised in Table 7.

Table 7. Displacement of the PZT disc with respect to the number of slots in a WEH end-cap

	Maximum displacement of piezoelectric disc		
End cap material	4 SLOTS	6 SLOTS	8 SLOTS
Steel	1.2626e-007 m	3.406e-007 m	2.4945e-006 m
Titanium	4.3792e-007 m	7.6044e-007 m	4.2336e-006 m
Brass	5.7952e-007 m	4.2268e-006 m	7.9538e-006 m

It can be clearly seen that for same materials and boundary conditions WEHs with larger numbers of slots have larger displacements, and thus a higher voltage output. This corresponds to the experimental results of the previous study (Yuan et al., 2009) performed for WW transducer. In addition, although the number of slots is changed, the performance pattern with respect to the different end-cap material still follows the one predicted for CEH.

6. Discussion of Results

In order to analyse the efficiency of a novel hybrid EHS a finite element model has been developed. It was created for a hybrid structure with nine CEHs sandwiched between two plates, with SMA wires providing the actuation in terms of compressive force. It was confirmed that the compressive force generated by the SMA wires was effectively transferred to the CEHs with an efficiency of almost 90%. Although some losses took place, the electrical energy converted compares favourably with other designs that have been developed previously.

To improve the efficiency of the design the number of SMA wires has been altered and a study of the influence of this on energy output was performed. It was shown that the amount of force relies on the number of SMAs used in the design due to the force distribution pattern along the top and bottom supporting plates, and a higher number of SMAs results in a higher voltage output. At the same time, according to Eq. (6), an increase in the peak output voltage results in a significant increase in power output (Figure 19).
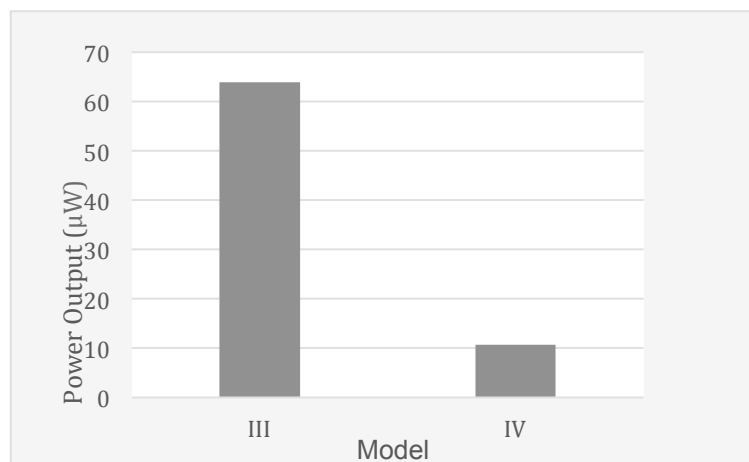

Figure 19. Total power output for models III and IV

A larger number of SMAs is also an advantage due to the heat transfer properties of such materials. A higher number of SMAs exhibits a larger surface area for the heat to be transferred to as compared with a smaller number of SMAs. The heat would also spread out to a larger number of SMA wires and therefore the actuation time could be decreased.

Following the success of the CEH application, the energy harvesting potential of a WEH was also demonstrated and shown to perform even better. A comparison between the results obtained and previously published was performed. It has also been shown that the energy output can be improved, effectively increasing the applied force or improving the piezoelectric strain constant of a piezoelectric disc. Additionally the effects of the end-cap material and the number of slots have been studied and it was concluded that an increase in their number would improve the performance, but would also challenge the material properties.

7. Conclusions

A novel hybrid EHS has been proposed and analysed in this paper. It has been demonstrated that the EHS is capable of converting enough energy to power a typical MEMS device.

A prototype based on a nine CEH array sandwiched between two steel plates has been proposed and considered in some detail.

A FEM was developed for the CEH following the dimensions of (Ren et al., 2010) with the purpose of verification of the FEM. The model performance was also tested in terms of its response to the change of the end-cap material, and the results confirmed previously published experimental results, specifically that the response of a CEH is dependent on the stiffness of the material (Young's Modulus).

 After verification of the FEM of the CEH, a FEM for the EHS was developed and analysed with respect to the location of SMA wires and force generated. It was found that models with SMA wires of a higher compressive capacity and with a higher number of SMA wires on each side guaranteed a better force distribution across both plates and provided a higher power output.

As a further optimisation of the EHS a novel Wagon Wheel design was explored in terms of its energy harvesting capabilities, by varying the material properties of the end-cap (brass, steel, titanium) and the number of slots. As expected, due to the increased displacement, an increase in the power output was achieved with the best performance for the material with the smallest Young's modulus and the larger number of slots. This corresponded to the experimental results of the previous study (Yuan et al., 2009) for the WW transducer.

Using previously published data and FEM developed, the analysis of the performance of the design suggested in Figure 12 for different number of SMA wires, a range of material of cymbal end-caps in the core of the EHS, and variable number of slots in wagon wheels to optimise the core cymbals, has confirmed that the design suggested has a strong potential for energy harvesting application. The EHS for the first time represents the combination of two smart materials for energy harvesting purposes in the environment with temperature changes. The combination of two smart materials in which they can compliment each other's properties to increase the energy output, and exploit a combination of physical effects, generally extending the area of application. The fact that the operating temperature of the SMA (the heating and cooling rate) depends on the composition of the SMA makes it possible to tune/train the SMA wires to be as sensitive as necessary for a specific application. The hybrid of

two smart materials suggested has a potential for miniaturisation which a step forward comparing to the work (Zakharov et al., 2012) and opens the door to applications in biomechanics. Further optimisation with a wagon wheel as an energy harvesting core gives an advantage in voltage output (Table 6) comparing to cymal design suggested in works in (Dogan et al., 1997; Kim et al., 2004; Berlincourt and Krueger, 2002) summarised in Table 2.

The most significant disadvantage of the novel design suggested is that the full EHS has to be perfectly tuned to guarantee the best performance possible. This means that the SMA wires have to be trained and tuned to operate at a certain frequency, wagon wheel cymbals in the core or the EHS ideally should operate at the resonance frequency which has to be the same for all cymbals in the array. This means that the design of the experimental prototype will face quite a few manufacturing challenges, fabrication of wagon wheel cymbals and the appropriate choice of SMA dimensions and alloy composition.

Further work will be also in the introduction of magnetically driven SMAs (MSMA), since MSMAs exhibit a higher operating frequency with a higher response from an externally applied magnetic field (Hubert et al., 2012).

8. References

Berlincourt DA, and Krueger HHA, Near.C. (2002) *Properties Of Morgan Electro Ceramic Ceramics*. Technical Report, Morgan Electro Ceramics.

Brandes EA (1983) *Smithell's Metals Reference Book*. 6th Ed. New York: Brandes, Butterworth.

Dogan A, Uchino K, and Newnham RE (1997) Composite piezoelectric transducer with truncated conical endcaps "cymbal". *IEEE Transactions on Ultrasonics, Ferroelectrics, and Frequency Control* 44(3): 597–605.

Dogan A, Uzgur E, Markley DC, et al. (2004) Materials for high performance cymbal transducers. *Journal of Electroceramics* 13: 403-407.

Dong S, Du XH, Bouchilloux PH, et al. (2002) Piezoelectric ring-morph actuators for valve application. *Journal of Electroceramics* 8: 155-161.

España FA, Balla VK, Bose S, et al. (2009) *'High Thermal Conductivity Coatings via LENS for Thermal Management Applications'*, School of Mechanical and Materials Engineering, Washington State University: Washington State University.

Feeney A, and Lucas M (2014) Smart cymbal transducers with nitinol end caps tunable to multiple operating frequencies. *IEEE Transactions on Ultrasonics, Ferroelectrics and Frequency Control* 61 (10): 1709-1719.

Fernandez JF, Dogan A, Fielding JT, et al. (1998) Tailoring the performance of ceramic-metal piezocomposite actuators, 'cymbals'. *Sensors and Actuators Part A* 65: 228-237.

Ganilova OA, Lucas M, Cardoni A (2011) An analytical model of cymbal transducer dynamics. Radial vibration of a piezoelectric disc. Proceedings of the

Institution of Mechanical Engineers. *Part C: Journal of Mechanical Engineering Science* 225:1077-1086.

Hubert A, Calchand N, Le Gorrec Y, et al. (2012). Magnetic Shape Memory Alloys as smart materials for micro-positioning devices. *Advanced Electromagnetics* 1(2): 75-84.

Jing-bo Y, Xiao-biao S, Tao X, et al. (2009) Energy harvesting with a slotted-cymbal transducer. *Journal Of Zhejiang University Science A* 10(1): 127-132.

Juuti J, Kordas K, Lonnakko R, et al. (2005) Mechanically amplified large displacement piezoelectric actuators. *Sensors and Actuators Part A* 120: 225-231.

Kim HW, Batra A, Sriya P, et al. (2004) 'Energy harvesting using a piezoelectric "Cymbal" transducer in dynamic environment', *Japanese Journal of Applied Physics* 43(1): 6178-6183.

Lam KH, Wang X, and Chan HLW (2006) Lead-free piezoceramic cymbal actuator. *Sensors and Actuators Part A* 125: 393-397.

Meyer RJ, Dogan A, Yoon C, et al. (2001) Displacement amplification of electroactive materials using the cymbal flextensional transducer. *Sensors and Actuators Part A* 87: 157-162.

Meyer RJ, Hughes JRWJ, Montogomery ThC, et al. (2002) Design of and fabrication improvements to the cymbal transducer aided by finite element analysis. *Journal of Electroceramics* 8: 163-174.

Morgan Advanced Material (2013) *Piezoelectric Ceramics*. [Brochure] Wrexham: Morgan Advanced Materials PLC.

Narayanan M, and Schwartz RW (2010) Design, fabrication and finite element modelling of a new wagon wheel flextensional transducer. *Journal of Electroceramics* 24(3): 205-213.

Ochoa P, Villegas M, Pons JL, et al. (2005) Tunability of cymbals as piezocomposite transducers. *Journal of Electroceramics* 14: 221-229.

Ostachowicz WM, Cartmell MP, Zak AJ (2001) Statics and dynamics of composite structures with embedded shape memory alloys. In: *Proceedings of the International conference on structural control and health monitoring* (SMART 2001), Warsaw, Poland, 22-25 May 2001.

Park EJ, Werner J, and Smith NB (2007) Ultrasound mediated transdermal insulin delivery in pigs using a lightweight transducer. *Pharmaceutical Research* 24(N7): 1396-1401.

Ren B, Or SW, Zhao X, et al. (2010) Energy harvesting using a modified rectangular cymbal transducer based on 0.71Pb(mg1/3Nb2/3)O3–0.29PbTiO3 single crystal. *Journal of Applied Physics* 107(3): 34501–34504.

SAES Group. *Smart Flex Springs and Wires*. [Brochure] s.l. : SAES Group, 2014.

Snyder B, Lee S, Smith NB, et al. (2006) Ferroelectric transducer arrays for transdermal insulin delivery. *Journal of Materials Science* 41: 211-216.

Sun CL, Lam KH, Chan HLW, et al. (2006) A novel drum piezoelectric-actuator. *Applied Physics Part A* 84: 385-389

Sun C, Shang G, Zhu X, et al. (2013) Modeling for piezoelectric stacks in series and parallel. In: *2013 Third International Conference on Intelligent System Design and Engineering Applications*, 16-18 January 2013, pp. 954–957.

Teh YH, and Featherstone R (2005) Experiments on the audio frequency response of shape memory alloy actuators. In: *Proceedings of 7th The Australasian Conference of Robotics and Automation*, Sydney, Australia, 5-7 December 2005.

Teh YH, and Featherstone R (2007) Frequency response analysis of shape memory alloy actuators. In: *International Conference on Smart Materials and Nanotechnology in Engineering (SMN 2007),* Harbin, China, 1-4 July.

Tressler JF, Alkoy S, Dogan A, et al. (1999) Functional composites for sensors, actuators and transducers. *Composites Part A Applied Science and Manufacturing* 30(4): 477–482.

Tressler JF, and Howarth TR (2002) A Comparison of the underwater acoustic performance of cymbal-based projectors to 1-3 piezocomposite materials. *Journal of Electroceramics* 8: 175-186.

Tressler JF, and Newnham RE (1997) Doubly resonant cymbal-type transducers. Special Issue Correspondence. *IEEE Transactions on Ultrasonics, Ferroelectrics, and Frequency Control* 44(N5): 1175-1177.

Wang XX, Or OW, Lam KH, et al. (2006) Cymbal actuator fabricated using (Na$_{0.46}$K$_{0.46}$Li$_{0.08}$) NbO$_3$ lead-free piezoceramic. *Journal of Electroceramics* 16: 385-388.

Wu L, Chure M, Wu K, et al. (2014) Voltage Generated Characteristics of Piezoelectric Ceramics Cymbal Transducer. *Journal of Materials Science and Chemical Engineering* 2: 32-37.

Yuan J, Shan X, Xie T, et al. (2009) Energy harvesting with a slotted-cymbal transducer. *Journal of Zhejiang University Sicence A* 10(8): 1187-1190.

Zakharov D, Lebede VG, Cugat O, et al. (2012). Thermal energy conversion by coupled shape memory and piezoelectric effects. *Journal of Micromechanics and Microengineering*, 22(9): 094005.

Zhang J, Hladky-Hennion AC, Hughes WJ, et al. (2001) A miniature class V flextensional cymbal transducer with directional beam patterns: the double-driver. *Ultrasonics* 39: 91-95.

Zhang J, Hughes WJ, Bouchilloux Ph, et al. (1999) A class V flextensional transducer: the cymbal. *Ultrasonics* 37: 387-393.